EINDHOVEN UNIVERSITY OF TECHNOLOGY

Department of Applied Physics

Modelling Pedestrian Dynamics on Curved Paths

3CBX0 - Bachelor End Project

A.D.S. Groot Zevert 1229971

dr. A. Corbetta

prof. F. Toschi

July 6, 2020

R-2015-SB

Abstract

The modelling of pedestrians is a very interesting and useful area of research for its various applications in real world problems. It can be used, for example, in the evacuations of buildings and the design of city roads. A way to model this is to compare pedestrians to active particles. Such a model has been made for pedestrians that follow a nearly straight path, but not when the path is curved. One approach to accomplish this is by choosing a path and defining it to be the result force free motion. With these curved paths as the basis, modelling components can be added to simulate trajectories. These components account for the random fluctuations in the movement, confining the pedestrian to the main path and adjusting the velocity such that it closes in on the natural walking speed. A comparison has been made between the model and people walking around on an elliptical trajectory to see how well the model performs.

Contents

1 Introduction

Modelling the behaviour of moving crowds is an interesting area of research, due to its wide range of real world applications. Two examples of this are evacuation dynamics [1] and the planning of cities [2, 3]. There are various ways to model pedestrian dynamics. May it be via statistical physics [4, 5], that may use a lattice like structures to determine the path of least resistance [6]. Or it can be done for large flows of crowds via fluid dynamics like equations [7, 8, 9]. These are all good approaches for crowds, though one can also consider the behaviour of pedestrians to resemble that of active particles [10]. This approach has already very promising results for diluted or even single pedestrian flows on nearly straight trajectories. But seeing as the trajectories of pedestrians are generally not straight, a generalisation to curved trajectories is proposed in this thesis. This is based on the concepts of force free motion, geodesics and stochasticity.

We start of with the conceptual theory behind the model, followed by some mathematical background. Then the model is put forth and its individual features presented. Thereafter, the model is compared to experimental data and some possible future improvements and applications are discussed.

2 Conceptual Theory

In this chapter the conceptual theory is presented as to improve the understanding and intuition of the subject.

If one were to let a ball roll on a flat surface and not interact with it, it would follow a straight line. This is because the motion of the ball is force free, the motion is governed by just Newtons second law without external forces present,

$$\vec{F} = m\vec{a} = 0, \tag{2.1}$$

where $\vec{F}, m, \vec{a}$ are the force, mass and acceleration respectively. Now a ball cannot deviate from the straight line without external forces present, but a human can walk in any path they wish. The difference between balls and humans in this case is that humans can force themselves internally to walk along an arbitrary path. Another thing that humans do is deviate from their path. One example that could cause this, of many, is making a small step to the side to keep balance. With these things in mind, we can try to model this behaviour. The first thing that comes the attention is the question of how the pedestrian that randomly deviates from the path, stays on the path. For this, a potential is introduced around the path. This is causes a force that pushes the pedestrian back to the main path. To see this in action, we go back to the ball. The ball is pushed along the straight path inside a kind of half pipe. Though the initial push is not perfect and it has a velocity a bit of to the side. In a perfect friction free world, the ball would now oscillate indefinitely around the main path as is illustrated in figure 2.1. This is comparable to a person that is walking along a path and accidentally steps to the side and then adjust their position again.

This works all really well for a straight path, but when modelling pedestrians, the same dynamics are needed around an arbitrary path. The first step is to chose a path for the model, a circle for example. Next, a potential perpendicular to the path can be constructed to confine the pedestrian. When now, the Newtonian dynamics are used to define the equations of motion as used with the straight line, the results in figure 2.2 are obtained. These would be the dynamics if a ball would have been pushed on the bottom of the circular potential well, perfectly tangential to the circle. As can be seen as the blue line in the figure, the ball does not follow the circle as desired. It oscillates around the circular path. The red line, indicates the bottom of he potential well on the circular path. This is a problem and calls for a new type of dynamics. Dynamics that are Newtonian like but instead of the force free paths being straight, they can be curved.

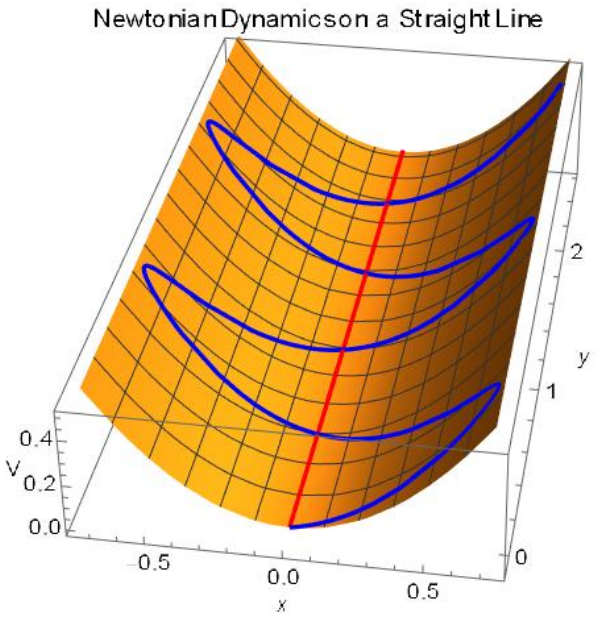

Figure 2.1: Newtonian dynamics on a straight path (red line) displaying oscillations (blue line) around the main path when the initial conditions are not along the main path. Both are imposed on the confining surface.

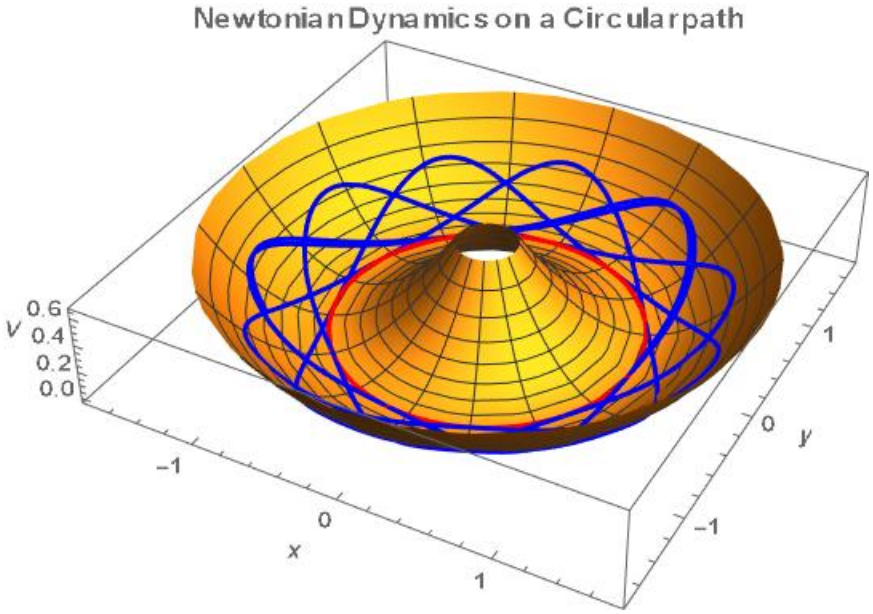

Figure 2.2: Newtonian dynamics on a circular path (red line) displaying oscillations (blue line) around the main path when the initial conditions are along the main path. Both are imposed on the potential surface.

To accomplish this, a branch of mathematics called differential geometry is used. These mathematics can describe the force free paths on curved surfaces, like a sphere. These paths are called geodesics and are the solution of the geodesic equation. This geodesic equation is what is needed to get curved force free motion. It is an equation that is an improved version of Newtons second law (2.1). The geodesic equation makes use of a covariant derivative. It can similarly to a normal derivative describe the change of something in a specific direction. The added bonus is that it also incorporates the effect of the change of the surface. This allows it to have circular force free paths, when using the right geometry. The geodesic equation is obtained when the covariant derivative of the velocity is taken in the direction of the velocity, that gives us the acceleration and therefore the new dynamics. An example of this can be

seen in figure 2.3, where a geodesic equation was made to create the circular trajectories where there is no acceleration in the radial of angular directions.

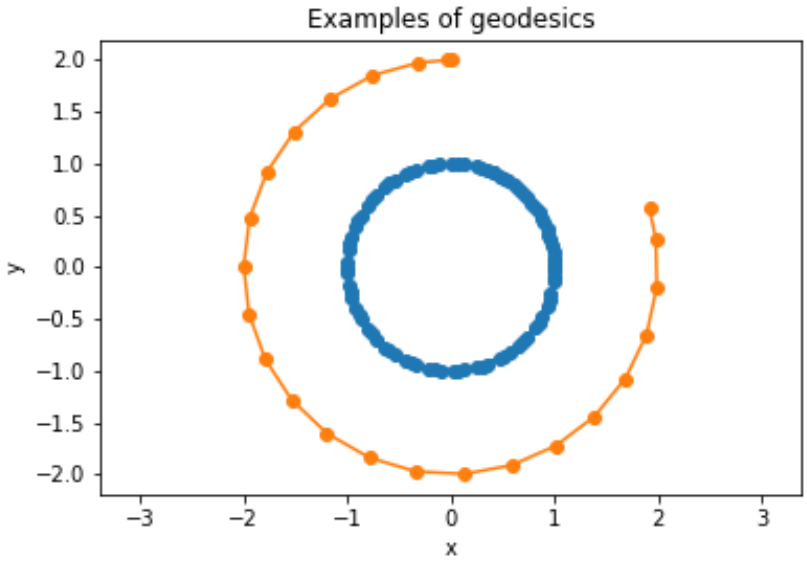

Figure 2.3: Two examples of geodesics derived using the geodesic equation, showing circular force free paths.

Using this new version of the equations of motion, a model can be constructed. In this model three components are used to describe the dynamics. A confining potential to keep pedestrians on the path, random fluctuations and an active friction term, that forces the pedestrian to walk with an average velocity.

3 Theoretical Background

In this section a mathematical background is given as a comprehensive overview of the theory that was used during the research. Both relevant concepts in differential geometry [11] and stochastic differential equations are discussed.

3.1 Differential Geometry

3.1.1 Curvilinear Coordinates

Curvilinear coordinates are a useful tool in describing a Euclidean space. Well known examples of curvilinear coordinates are polar and spherical coordinates in $\mathbb{R}^2$ and $\mathbb{R}^3$ respectively. Consider the point described by the vector $\vec{r} = (x, y, z)$ in $\mathbb{R}^3$ or $\vec{r} = x^i \boldsymbol{e_i}$ in $\mathbb{R}^n$, where $\boldsymbol{e_i}$ is the basis and the Einstein summation convention is implied in the latter expression. This point can also be described by the curvilinear coordinates q^i. A mapping, f^i, between the Cartesian and curvilinear coordinates can be made as

$$x^i = f^i(q^1, q^1, ..., q^n), \tag{3.1}$$

and likewise the inverse mapping, g^i, as

$$q^i = g^i(x^1, x^1, ..., x^n). \tag{3.2}$$

With these transformations, the covariant basis vectors of the curvilinear coordinate system, $\boldsymbol{e_i}$, can be defined based on the Cartesian basis vectors

$$\boldsymbol{e_i} = \frac{\partial \vec{r}}{\partial q^i}. \tag{3.3}$$

The length of these vectors are called scale factors or Lamé coefficients and are generally denoted by h_i. They can be used for defining the gradient in curvilinear coordinates,

$$\nabla\phi = \frac{1}{h_i}\frac{\partial\phi}{\partial q^i}\boldsymbol{e_i}. \tag{3.4}$$

3.1.2 The Metric Tensor

With these basis vectors, the metric tensor can be defined,

$$g_{ij} = \boldsymbol{e_i} \cdot \boldsymbol{e_j}. \tag{3.5}$$

This tensor defines the line elements of the space. It also has an inverse, namely

$$g^{ij} = g_{ij}^{-1}, \tag{3.6}$$

with the property that

$$g^{ik}g_{kj} = \delta^i_j, \tag{3.7}$$

where δ^i_j is the Kronecker delta. The metric tensor can also be used to raise or lower indices of basis vectors e.g.

$$\mathbf{e^j} = g^{ij}\mathbf{e_i} \text{ and } \mathbf{e_j} = g_{ij}\mathbf{e^i} \tag{3.8}$$

3.1.3 Covariant Derivative

Now that there is a metric tensor, a notion of a derivative is required, this comes in the form of the covariant derivative. This covariant is a generalisation of the normal directional derivative, that is introduced to account for the changing coordinate vectors. The covariant derivative of $\vec{u}$ in the direction of $\vec{v}$ with a basis $\boldsymbol{e_i}$ is defined as

$$\nabla_{\vec{v}}\vec{u} = v^j u^i \Gamma^k_{ij}\mathbf{e}_k + v^j\frac{\partial u^i}{\partial x^j}\mathbf{e}_i. \tag{3.9}$$

Where Γ^k_{ij} are the connection coefficients or the Christoffel symbols of the second kind, note that

$$\Gamma^k_{ij} = (\nabla_{\boldsymbol{e_i}}\boldsymbol{e_j})\boldsymbol{e^k} = \frac{\partial \boldsymbol{e_i}}{\partial x^j}\boldsymbol{e^k}. \tag{3.10}$$

3.1.4 Parallel Transport and the Geodesic Equation

The connection as defined in the previous section can be used for transportation on the manifold via parallel transport. A manifold is a space that can locally be represented by a Euclidean space. Parallel transport of a vector $\vec{v}$ along a vector field $\vec{u}$ is defined as

$$\nabla_{\vec{u}}\vec{v} = 0. \tag{3.11}$$

This equation makes sure that the vector $\vec{u}$ stays parallel with respect to the connection while transported over the manifold.

Geodesics on a smooth manifold are the curves of no acceleration and thus force free. These curves generalise the concept of the 'straightest' path. More formally, a geodesic is a curve, say $x(t)$, which preserves the tangent vector during parallel transport, i.e.

$$\nabla_{\dot{x}}\dot{x} = 0, \tag{3.12}$$

where $\dot{x} = \frac{dx}{dt}$. This equation, when written out, results in the geodesic equation

$$\ddot{x}^k + \Gamma^k_{ij}\dot{x}^i\dot{x}^j = 0 \tag{3.13}$$

3.1.5 Pull-Back and Push-Forward

To easily change between two coordinate systems, the pull-back and push-forward are introduced. With these one can move between two manifolds, say M and N, by use of a linear mapping $\phi : M \to N$ called the pull back. When ϕ is a diffeomorphism, the push forward is given by its inverse ϕ^{-1}. These mappings can also be used to pull-back or push-forward vectors, denoted by ϕ_* and ϕ_*^{-1} respectively. To carry out the calculations, the Jacobian of the mapping ϕ is used, J_ϕ. To give an example, if there is a vector v on the tangent space of M, TM, it can be pulled back to the tangent space on N, TN, as follows,

$$v' = \phi_*(v) = J_\phi v. \tag{3.14}$$

Furthermore, with the use of the pull back of the vectors, the connection can be transferred from one manifold to another. Let ∇ denote a connection on the manifold N and w, v vectors on TN.Then a connection on M, say $\tilde{\nabla}$, can be given by

$$\tilde{\nabla}_w v = \phi_* \left(\nabla_{\phi_*^{-1}(w)} \phi_*^{-1}(v) \right) \tag{3.15}$$

3.1.6 Example: Polar Coordinates

Polar coordinates are very commonly used, like in this research project, and are therefore make an excellent example. In $\mathbb{R}^2$, $(x^1, x^2) = (x, y)$ and $(q^1, q^2) = (r, \theta)$. The transformation, $\phi : q \to x$, and its inverse, $\phi^{-1} : x \to q$, are given by

$$\phi : \begin{cases} x = r\cos(\theta) \\ y = r\sin(\theta) \end{cases} \quad \text{and} \quad \phi^{-1} : \begin{cases} r = \sqrt{x^2 + y^2} \\ \theta = \arctan\left(\frac{y}{x}\right) \end{cases} . \tag{3.16}$$

With this, the basis vectors can be calculated

$$\boldsymbol{e_r} = \frac{\partial \vec{r}}{\partial r} = \cos(\theta)\boldsymbol{e_x} + \sin(\theta)\boldsymbol{e_y}, \tag{3.17}$$

$$\boldsymbol{e_\theta} = \frac{\partial \vec{r}}{\partial \theta} = -r\sin(\theta)\boldsymbol{e_x} + r\cos(\theta)\boldsymbol{e_y}. \tag{3.18}$$

With these newfound basis vectors the metric tensor can be calculated,

$$g_{ij} = \boldsymbol{e_i} \cdot \boldsymbol{e_j} = \begin{bmatrix} 1 & 0 \\ 0 & r^2 \end{bmatrix}. \tag{3.19}$$

Next, the Christoffel symbols can be calculated,

$$\Gamma^r_{\theta\theta} = -r \ , \ \Gamma^\theta_{r\theta} = \Gamma^\theta_{\theta r} = \frac{1}{r}, \tag{3.20}$$

the rest of the symbols are 0. Now the geodesic equations can be easily calculated and result in

$$\ddot{r} - r\dot{\theta}^2 = 0, \tag{3.21}$$

$$\ddot{\theta} + \frac{2\dot{r}\dot{\theta}}{r} = 0. \tag{3.22}$$

Which, when solved, give the equation for a straight line,

$$r = \frac{1}{a\cos\theta + b\sin\theta}, \tag{3.23}$$

with a and b integration constants.

3.2 Stochastic Differential Equations

When trying to model the dynamics of a pedestrian the base model consist of an ordinary differential equation (ODE) e.g. the geodesic equation discussed in section 3.1.4. This makes for a very fine first model, but real life is not as perfect. Therefore, an extra stochastic term needs to be added to the model. This transforms the ODE into a stochastic differential equation (SDE). The fundamentals of these equations will be discussed in this section.

3.2.1 Wiener Process

To start of the discussion about stochastic differential equation, a stochastic process is needed. Here we discuss a Wiener process, though also called Brownian motion. A Wiener process $W(t)$ has the following properties

- $W(t=0)=0$,
- W has independent increments, it is uncorrelated,
- The distribution of W is a Gaussian distribution centred at 0 i.e. $W(t)-W(0)\sim\mathcal{N}(0,t)$,
- W is continuous in time.

3.2.2 Construction of an SDE

The starting point of constructing and SDE [12, 13] is an ODE, for example take the following ODE:

$$\frac{\mathrm{d}x(t)}{\mathrm{d}t}=a(t)x(t),\quad \mathrm{d}x(t)=a(t)x(t)\mathrm{d}t, \tag{3.24}$$

where x is the unknown function and a and arbitrary function of t. When supplied with the initial condition $x(0)=x_0$, the equation above can be written in integral form like

$$x(t)=x_0+\int_0^t a(s)x(s)\mathrm{d}s. \tag{3.25}$$

Now suppose the prefactor a becomes a stochastic parameter, with white Gaussian noise $\eta(t)$, random noise with a Gaussian distribution centred at 0,

$$a(t)=f(t)+g(t)\eta(t). \tag{3.26}$$

Now equation (3.24) becomes,

$$\frac{\mathrm{d}X(t)}{\mathrm{d}t}=f(t)X(t)+g(t)X(t)\eta(t), \tag{3.27}$$

where $X(t)$ is now a random variable. This can also be put into differential form, like the ODE,

$$\mathrm{d}X(t)=f(t)X(t)\mathrm{d}t++g(t)X(t)\mathrm{d}W(t). \tag{3.28}$$

Note that $\eta(t)\mathrm{d}t$ is written as $\mathrm{d}W(t)$, the derivative of Brownian noise [14]. Note that $(\mathrm{d}W(t))^2=\mathrm{d}t$. Same as before, this can now be written in integral form, with $X(0)=X_0$,

$$X(t)=X_0+\int_0^t f(s)X(s)\mathrm{d}s+\int_0^t g(s)X(s)\mathrm{d}W(s). \tag{3.29}$$

The latter integral is a stochastic integral.

3.2.3 The Itô Integral

A stochastic integral like

$$S=\int_0^T g(t)\mathrm{d}W(t), \tag{3.30}$$

can be defined for by a Riemann Sum. Using N points in time, $0=t_0<t_1<t_2<...<t_{N-1}<t_N<T$, the Riemann Sum can be written as

$$S_N=\sum_{i=1}^{N} g(t_{i-1})(W(t_i)-W(t_{i-1})), \tag{3.31}$$

with $N\to\infty$. S is called the Itô integral of $g(t)$ with respect to $W(T)$.

3.2.4 The Stratonovich Integral

It is noteworthy to mention that the Itô integral is not the only way to describe stochastic integrals. There is another integral called the Stratonovich integral which can be easier to work with in some cases, as it defined to follow the ordinary chain rule. The integral with respect to X takes the form of

$$\int_0^T X(t) \circ \mathrm{d}W. \tag{3.32}$$

The Stratonovich integral can be represented in terms of the Itô integral

$$\int_0^t X(s) \circ dY(s) = \int X(s) dY(s) + \frac{1}{2}[X, Y]_t^c, \tag{3.33}$$

where $[X, Y]_t^c$ denotes the quadratic cross-variation process of X and Y. The very compelling property that the Stratonovich integral obeys the chain rule makes it very useful when expressing stochastic processes on non-Euclidean manifolds.

3.2.5 Itô's Lemma

Itô calculus is an extension on normal calculus that makes it possible to describe processes dependent on Brownian motion. This extension though, changes a well known rule of calculus, namely the chain rule. Whereas normally it would go as follows for $f = f(x, y)$,

$$\mathrm{d}f = \frac{\partial f}{\partial x}\mathrm{d}x + \frac{\partial f}{\partial y}\mathrm{d}y, \tag{3.34}$$

it does not hold for stochastic processes. Consider $f = f(t, W)$, it can be shown when expanding $\mathrm{d}f$ using a Taylor expansion.

$$\mathrm{d}f = \frac{\partial f}{\partial t}\mathrm{d}t + \frac{\partial f}{\partial W}\mathrm{d}W + \frac{1}{2}\frac{\partial^2 f}{\partial t^2}(\mathrm{d}t)^2 + \frac{\partial^2 f}{\partial t \partial W}\mathrm{d}t\mathrm{d}W + \frac{1}{2}\frac{\partial^2 f}{\partial W^2}(\mathrm{d}W)^2 + \text{ higher order terms.} \tag{3.35}$$

We now only consider the first order terms in $\mathrm{d}t$.

$$\mathrm{d}f = \frac{\partial f}{\partial t}\mathrm{d}t + \frac{\partial f}{\partial W}\mathrm{d}W + \frac{1}{2}\frac{\partial^2 f}{\partial W^2}(\mathrm{d}W)^2 \tag{3.36}$$

When this is rewritten using $(\mathrm{d}W)^2 = \mathrm{d}t$, the renewed chain rule is obtained, called Itô's Lemma,

$$\mathrm{d}f = \left(\frac{\partial f}{\partial t} + \frac{1}{2}\frac{\partial^2 f}{\partial W^2}\right)\mathrm{d}t + \frac{\partial f}{\partial W}\mathrm{d}W. \tag{3.37}$$

3.2.6 Coordinate Change of Noise

Gaussian white noise is well defined when using a Cartesian coordinate system, though not necessarily in generalised coordinate systems. Luckily, the noise can be transformed by use of a coordinate transformation [15]. This is not a normal transformation when one is using Itô calculus, due to Itô's lemma.

When taking the change to polar coordinates for example given by equation (3.16). Normally the differentials would be given by

$$\begin{aligned} \mathrm{d}x &= \cos\theta \mathrm{d}r - r\sin\theta \mathrm{d}\theta \\ \mathrm{d}y &= \sin\theta \mathrm{d}r + r\cos\theta \mathrm{d}\theta \end{aligned}, \tag{3.38}$$

But now, the transformation of the noise goes like

$$\begin{aligned} \mathrm{d}x &= \cos\theta \mathrm{d}r - r\sin\theta \mathrm{d}\theta - \tfrac{1}{2}r\cos\theta(\mathrm{d}\theta)^2 \\ \mathrm{d}y &= \sin\theta \mathrm{d}r + r\cos\theta \mathrm{d}\theta - \tfrac{1}{2}r\sin\theta(\mathrm{d}\theta)^2 \end{aligned}. \tag{3.39}$$

The $(\mathrm{d}\theta)^2$ is there because it has a term proportional to $(\mathrm{d}W)^2$ and the $(\mathrm{d}r)^2$ is not there because, in this particular case, $\frac{\partial^2 \phi}{\partial r^2} = 0$. Both $\mathrm{d}r$ and $\mathrm{d}\theta$ have the structure of equation (3.37). It is interesting to compare this to the Stratonovich SDE. It obeys the rules of classical calculus, which cause the transformation between coordinates to behave like normal,

$$\begin{pmatrix} \mathrm{d}x \\ \mathrm{d}y \end{pmatrix} = J_\phi \begin{pmatrix} \mathrm{d}r \\ \mathrm{d}\theta \end{pmatrix}, \tag{3.40}$$

making it an easier tool for calculations. It is possible, and perhaps simpler, to convert the SDE in the Stratonovich sense and then convert it back into the Itô representation in the curvilinear coordinate system. This conversion can be done in arbitrary coordinates with a simple conversion rule. Take the general Itô and Stratonovich SDEs

$$\mathrm{d}X_i = a_i \mathrm{d}t + \sum_{j=1}^{d} B_{ij} \mathrm{d}W_j, \tag{3.41}$$

$$\mathrm{d}X_i = a_i^s \mathrm{d}t + \sum_{j=1}^{d} B_{ij}^s \circ \mathrm{d}W_j, \tag{3.42}$$

with $i = 1, ..., d$. Then the conversion between them is given by,

$$a_i = a_i^s + \frac{1}{2} \sum_{j=1}^{d} \sum_{k=1}^{d} \frac{\partial B_{ij}^s}{\partial q_k} B_{kj}^s \quad \text{with} \quad B_{ij}^s = B_{ij}. \tag{3.43}$$

3.2.7 Euler–Maruyama method

When numerically solving the SDEs, one simple method often used is the Euler-Maruyama scheme or stochastic Euler scheme [16, 17]. This method is based on the Euler method for ODEs. The extension to SDEs was first studied by Maruyama [18] and can be used to solve SDEs in Itô form. The method is briefly discussed here to illustrate how an SDE can be solved numerically.

The Euler-Maruyama method can be used to solve equations of the type

$$\mathrm{d}X(t) = a(t, X(t))\mathrm{d}t + b(t, X(t))\mathrm{d}W. \tag{3.44}$$

The scheme itself uses a partition on the time interval $[0, T]$ of n equal subintervals with $\Delta t = T/n$. Then the solution can be defined recursively by

$$X_{n+1} = X_n + a(t_n, X_n)\Delta t + b(t_n, X_n)\Delta W_n, \tag{3.45}$$

with $\Delta W_n = W_{t_{n+1}} - W_{t_n}$. This concept can be generalised to multidimensional SDEs of dimension d,

$$dX_i(t) = a_i(t, X(t))dt + \sum_{k=1}^{d} B_{ik}(t, X(t))dW_k(t), \quad X_i(0) = X_{i,0}, \tag{3.46}$$

With vectors X, a, W and the correlation matrix B. Note that for an independent Wiener process B becomes a diagonal matrix. The scheme to numerically solve these equations is

$$X_i^{(n+1)} = X_i^{(n)} + a_i\left(t^{(n)}, X^{(n)}\right) h + \sum_{k=1}^{d} B_{ik}\left(t^{(n)}, X^{(n)}\right) \Delta W_k^{(n)}. \tag{3.47}$$

This method is easy to implement, but not a accurate method. It has strong order convergence of 0.5 [19]. Stronger methods have been developed by, for example by Rößler [20].

4 Mathematical Model

In this chapter the mathematical model is introduced. The model is introduced component wise. Alongside this model, a working example of a circular trajectory is considered to help illustrate the model and its components. The model is made using python, for more details, see the appendix A.

4.1 Base Equations

The first goal for describing pedestrian dynamics on a curved path is to make the basis equations. When considering the straight path trajectory [10], the first part of the equations were

$$\ddot{x} = 0 \quad \text{and} \quad \ddot{y} = 0. \tag{4.1}$$

This can be generalised to our path in curvilinear coordinates (q_1, q_2), where on of the coordinate lines is the path itself, say q_1. Then, the equations can be written as,

$$\ddot{q}_1 = 0 \quad \text{and} \quad \ddot{q}_2 = 0. \tag{4.2}$$

These make sure that there is no deviation from the desired path and the velocity stays constant. However this can be modified to ones wishes as to conserve quantities otherwise not conserved. To make the equations fit to the structure of a Langevin equation the equations are rewritten in vector form with $\vec{q}$, $\vec{u}$ the coordinates and their velocities and where ∇ denotes the covariant derivative.

$$\begin{cases} \dot{\vec{q}} = \vec{u} \\ \nabla_{\vec{u}}\vec{u} = 0 \end{cases}. \tag{4.3}$$

The connection can, as described in section 3.1.5, be pulled back to Cartesian coordinates, where the modelling components have previously been defined and work. The other option is to describe the modelling components in the curvilinear coordinate system, there should be no difference in dynamics. The choice would be up to preference.

As an example, take a circular trajectory described in polar coordinates (r, θ). The equations as described above would result in

$$\begin{cases} \ddot{r} = 0 \\ \ddot{\theta} = 0 \end{cases}. \tag{4.4}$$

This is feasible if the pedestrian stays on the circle of if the deviations are very small, but when the deviations become very large, or the path not described by one single coordinate line, the equations do not work as intended. This is due to the fact that the fact that $\dot{\theta} = constant$. This means that if the pedestrian moves to a larger radius the speed would increase. This, in turn, is due to the circumference of the circle, which increases with r, all the while the time in which the full circle is travelled remains the same. This can be seen in figure 4.4a where the radial spacing in the spiral remains equidistant and in figure 4.4c where the velocity keeps increasing.
A better option would be if the angular momentum, $r\dot{\theta}$, would be conserved,

$$\begin{cases} \ddot{r} = 0 \\ \frac{\mathrm{d}}{\mathrm{d}t}(r\dot{\theta}) = 0 \end{cases}. \tag{4.5}$$

Then, the norm of the velocity would remain constant at all radii, as can be seen in figure 4.4b and figure 4.4d. Here it can be seen that the norm of the velocity remains constant. Because equations (4.5) are not of the same form as equations (4.2), the Christoffel symbols associated with these geodesic equations are not all zero. The ones that are non-zero can easily be read off if the derivatives are worked out,

$$\ddot{\theta} + \frac{\dot{r}\dot{\theta}}{r} = 0, \tag{4.6}$$

implying,

$$\Gamma^{\theta}_{r\theta} = \Gamma^{\theta}_{\theta r} = \frac{1}{2r}. \tag{4.7}$$

This angular momentum conserving connection can be pulled back to Cartesian coordinates (x, y),

$$\begin{cases} \ddot{x} - \frac{y\dot{x}\dot{y}}{x^2+y^2} + \frac{x(\dot{y})^2}{x^2+y^2} = 0 \\ \ddot{y} + \frac{y(\dot{x})^2}{x^2+y^2} - \frac{x\dot{x}\dot{y}}{x^2+y^2} = 0 \end{cases}. \tag{4.8}$$

The model was tested for the circular example with these Cartesian equations.

4.2 Confinement

Next to be able to keep the pedestrian on its path, the confining potential. It is a parabolic potential around the the main path. When working in these curvilinear coordinates, it can be easily constructed. Let $q_1 = k$, where k is a constant, be the coordinate line that forms the path. Then the potential V is described by,

$$V = \alpha(q_1 - k)^2, \tag{4.9}$$

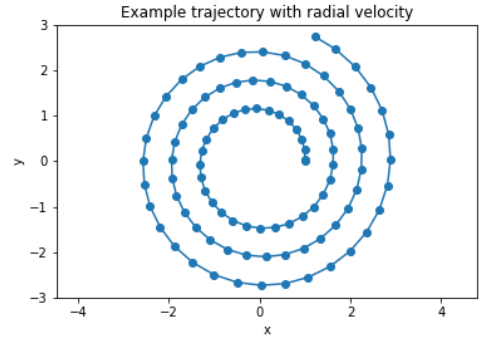

(a) a trajectory where $\dot{r} \neq 0$ and the angular velocity is conserved

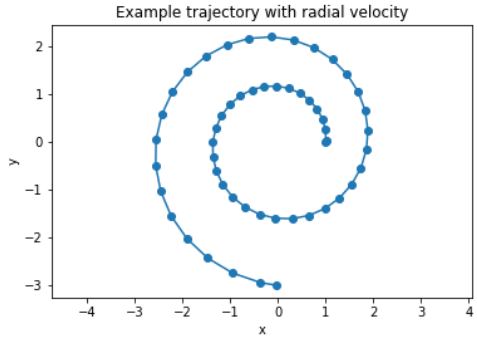

(b) a trajectory where $\dot{r} \neq 0$ and the angular momentum is conserved

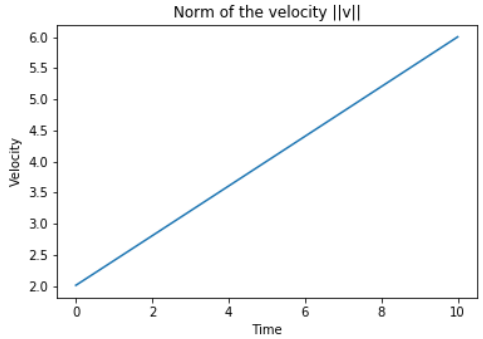

(c) The norm of the velocity when angular velocity is conserved

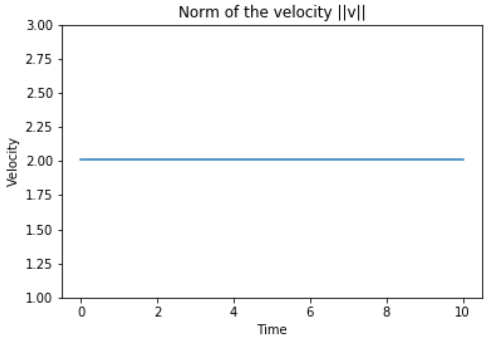

(d) The norm of the velocity when angular momentum is conserved

Figure 4.4: Four plots showing the difference between the equations that conserve the angular velocity and the angular momentum.

where α is a parameter that indicates the stiffness of the potential. The potential can be implemented into the geodesic equation like in normal Newtonian dynamics with the use of the gradient function ∇,

$$\nabla_{\vec{u}}\vec{u} = -\nabla V \tag{4.10}$$

The gradient used is the normal gradient as discussed in section 3.1.1. This gives the total set of equations up to this point

$$\begin{cases} \dot{\vec{x}} = \vec{u} \\ \nabla_{\vec{u}}\vec{u} + \nabla V = 0 \end{cases}. \tag{4.11}$$

In the working example of the circle, the potential to zero at $r = R$, on the path. The potential then is,

$$V(r) = \alpha(r - R)^2 = \alpha(\sqrt{x^2 + y^2} - 1)^2. \tag{4.12}$$

The gradient of the potential can either be taken in Cartesian or polar coordinates using equation (3.4). This results in

$$\nabla V = \begin{cases} 2(r-1)\boldsymbol{e_r} \\ 0 \end{cases} = \begin{cases} 2\alpha(\sqrt{x^2+y^2} - 1)\frac{x}{\sqrt{x^2+y^2}}\boldsymbol{e_x} \\ 2\alpha(\sqrt{x^2+y^2} - 1)\frac{y}{\sqrt{x^2+y^2}}\boldsymbol{e_y} \end{cases} \tag{4.13}$$

When simulated, the pedestrian gets pushed onto the desired trajectory. This can be seen in figures 4.5a and 4.5b. There the pedestrian starts at an inner or outer radius and gets pushed towards the desired path, denoted by "reference circle", by the potential.

4.3 Active Friction

The next modelling component to be added it the active friction term. This term pushes the pedestrian to walk at a desired velocity. It is introduced here as follows,

$$\nabla_{\vec{u}}\vec{u} + \frac{\vec{v}_d - \vec{u}}{\tau} = 0. \tag{4.14}$$

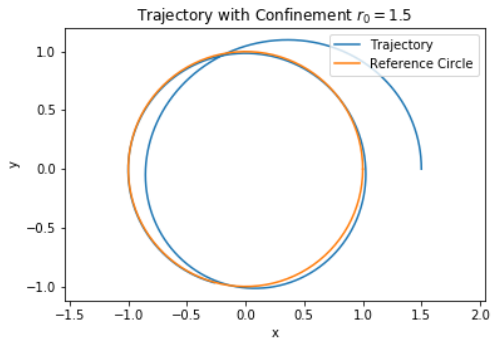

(a) The trajectory with the confining potential implemented, initial radius $r_0 = 1.5$.

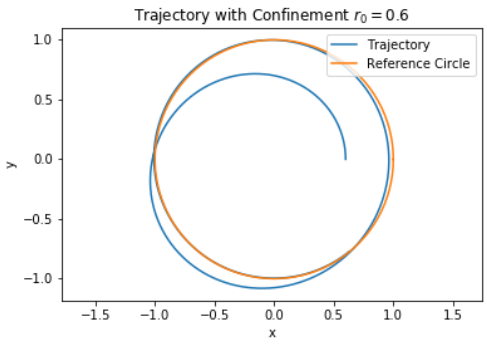

(b) The trajectory with the confining potential implemented, initial radius $r_0 = 0.6$.

Figure 4.5: The implementation of the confinement into the model. Where the (blue line) gets pushed onto the circular path (orange line).

Where $\vec{v_d}$ is the desired velocity and τ a time parameter. To be able to always have a well defined velocity along the path, the velocity has to be transported parallel to the path. This can also be done by the covariant derivative,

$$\nabla_{\vec{u}} \vec{v}_d = 0, \tag{4.15}$$

adding two more equations giving a total of six.

$$\begin{cases} \dot{\vec{q}} = \vec{u} \\ \nabla_{\vec{u}} \vec{u} + \frac{\vec{v_d} - \vec{u}}{\tau} + \nabla V = 0 \\ \nabla_{\vec{u}} \vec{v_d} = 0 \end{cases} \tag{4.16}$$

The workings and effect on the trajectory can be seen in figures 4.6a and 4.6b. Here the parallel transport of $\vec{v}_d$ and the walking velocity approaching $\vec{v}_d$ can be seen for the dynamics on the circle.

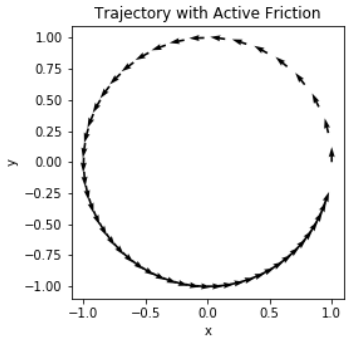

(a) The trajectory with the active friction at work, the arrows denote the desired velocity vector and are equally space in time. This shows the active friction at work.

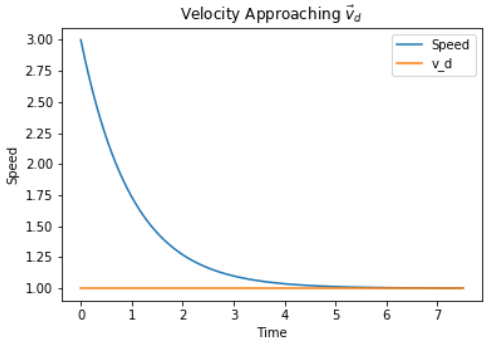

(b) The velocity (blue) approaching and reaching the desired velocity (orange) in time.

Figure 4.6: The implementation of the active friction at work

In the running example of polar coordinates, the two terms of the active friction are

$$\frac{v_{dr} - \dot{r}}{\tau} \quad \text{and} \quad \frac{v_{d\theta} - r\dot{\theta}}{\tau}, \tag{4.17}$$

where v_{dr} and $v_{d\theta}$ are the two components of $\vec{v}_d$. Note that there is an $r\dot{\theta}$ term as that is the appropriate tangential velocity term. It is equally well described in Cartesian coordinates as

$$\frac{v_{dx} - \dot{x}}{\tau} \quad \text{and} \quad \frac{v_{dy} - \dot{y}}{\tau}, \tag{4.18}$$

with v_{dx} and v_{dy} the components of $\vec{v}_d$.

4.4 Noise

The final part of the model is the implementation of the noise. This is there to account for the random fluctuations in the walking behaviour. The noise that is used is Gaussian white noise, which is random noise with a Gaussian distribution centred at 0 it is also the derivative of Brownian motion [14]. The SDE that is obtained is interpreted according to Itô calculus discussed in section 3.2. The equations of motion then become,

$$\nabla_{\vec{u}}\vec{u} + \frac{\vec{v_d} - \vec{u}}{\tau} + \nabla V + \sigma \dot{W}_{\vec{x}} = 0, \tag{4.19}$$

where $\dot{W}_{\vec{x}}$ denotes the derivative of Brownian motion and σ a scale factor. Note that the noise has to be transformed from Cartesian coordinates according to section 3.2.6.

The trajectories that can be calculated from this, figures 4.7a and 4.7b, are showing oscillatory behaviour around the mean path. As is both expected and desired from the model.

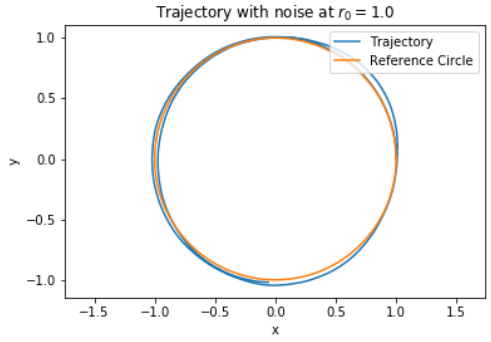

(a) The trajectory with noise, oscillating around the reference circle.

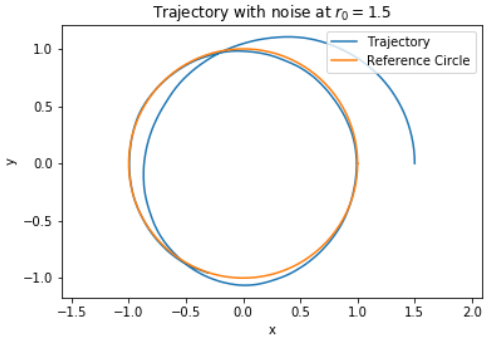

(b) Trajectory with noise starting outside the circle and being pushed in by the confinement.

Figure 4.7: Two single simulations trajectories of the model.

4.5 Rescaling the Desired Velocity

A problem with this model thus far is that the transport of the desired velocity along the path with confinement and the noise is not working as wanted.The problem here is that, during the transport, the length of $\vec{v}_d$ in not preserved, as can be seen in figures 4.8a and 4.8b. To account for this, the initial vector $v_{d,i}$ is used to rescale the transported vector, $\vec{v}_d \rightarrow v_{d,i}\frac{\vec{v}_d}{||\vec{v}_d||} = \vec{v}_d\prime$. This corrects the length and preserves the direction of the vector. The result can be seen in figure 4.9, where the desired velocity stays constant and the speed oscillates around it.

$$\begin{cases} \dot{\vec{q}} = \vec{u} \\ \nabla_{\vec{u}}\vec{u} + \frac{\vec{v_d}\prime - \vec{u}}{\tau} + \nabla V = 0 \\ \nabla_{\vec{u}}\vec{v_d} = 0 \end{cases} \tag{4.20}$$

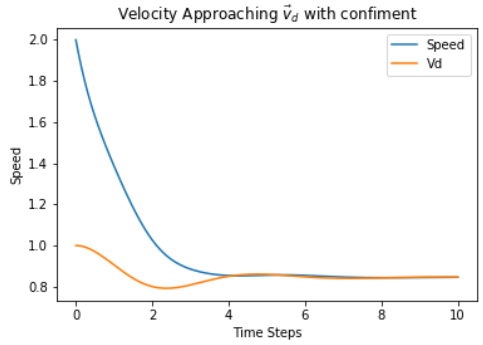

(a) The velocity approaching the desired velocity with the confinement.

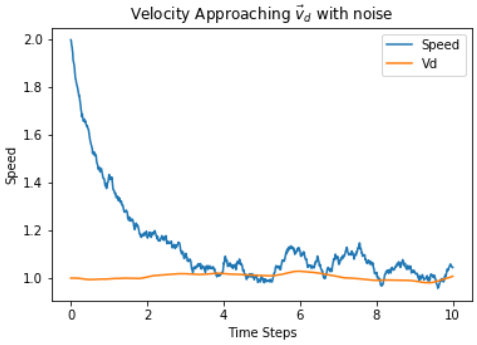

(b) The velocity approaching the desired velocity with noise added in the model.

Figure 4.8: The transport of $\vec{v}_d$ not going as desired.

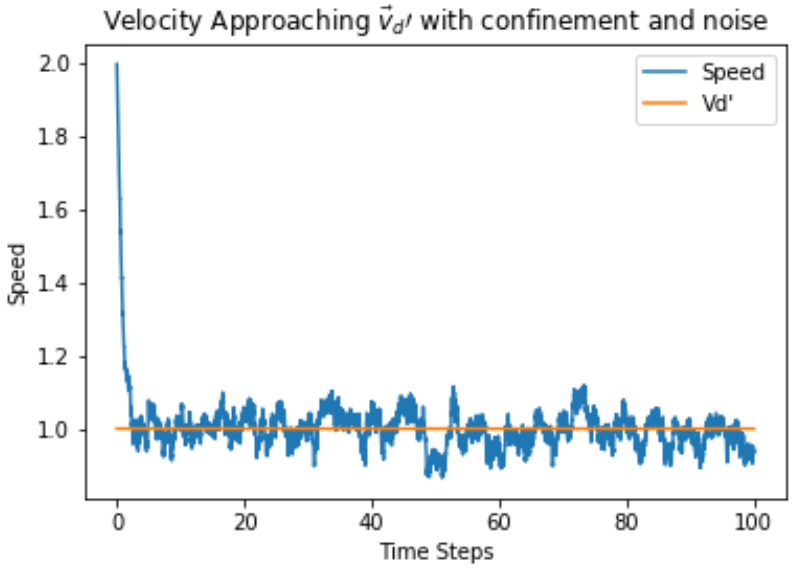

Figure 4.9: The velocity approaching the desired velocity, the latter of which now has a predetermined constant size.

All of these modelling components combined give in total 6 equations that govern the motion. In the working example of polar coordinates these are

$$\begin{cases} \dot{r} = u \\ \dot{\theta} = v \\ \dot{u} + \frac{v_{dr}{}' - u}{\tau} + \alpha(r-1) + \sigma W_r = 0 \\ r\dot{v} + uv + \frac{v_{d\theta}{}' - rv}{\tau} + \sigma W_\theta = 0 \\ \dot{v}_{dr} = 0 \\ \dot{v}_\theta = \frac{1}{2r} v_{dr} v + \frac{1}{2r} v_{d\theta} u \end{cases}, \tag{4.21}$$

where W_r and W_θ are the transformed Gaussian white noise components. These can, of course, be written in Cartesian form as well. With these equations of motion, many trajectories of all kinds can be simulated. In the next chapter, many simulations of a circular trajectory will be made.

5 Simulations

To make sure the model is behaving like intended, simulations have been carried out to find average trajectories, distributions of the radius and velocity.

5.1 Simulations on a Circle

The simulations of this model have been carried out in a python code. The model described in Cartesian coordinates has been used to verify the model. The first thing to do is to simulate a lot of trajectories, 20 of those can be seen in figure 5.10. The set of simulated trajectories consists of 1000 trajectories, all simulated for 250 seconds with 5000 time steps in total. The initial conditions are

$$[x_0, y_0, u_0, v_0, v_{dx,i}, v_{dy,i}] = [1, 0, 0, 1, 0, 1], \tag{5.1}$$

The initial x and y position, velocities and the desired velocities.

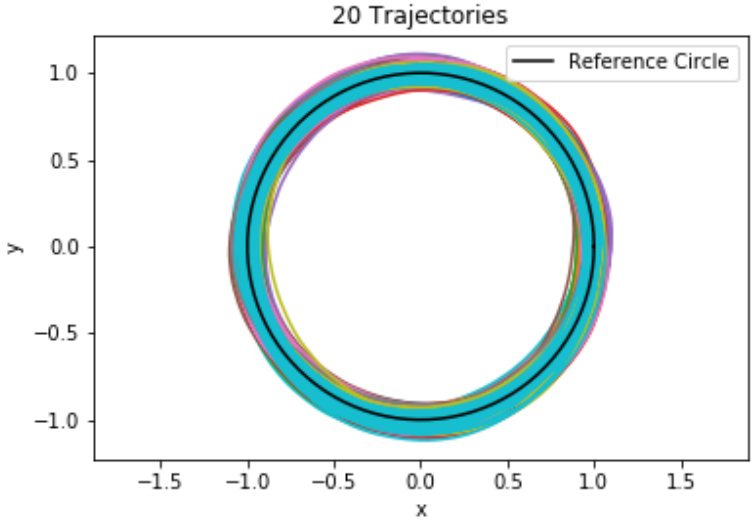

Figure 5.10: 20 simulated trajectories plotted on top of one another together with a reference circle (black line) to indicate the desired path. The initial conditions are as described above. Further parameters: $\alpha = 1$, $\tau = 1$ and $\sigma = 0.07$.

As can be seen in the figure, the trajectories stay nicely confined near the desired path. Due to the long simulation times, each pedestrian goes several times around the circle. The radial distribution of the simulations can be seen in the histograms in figures 5.11a and 5.12b.

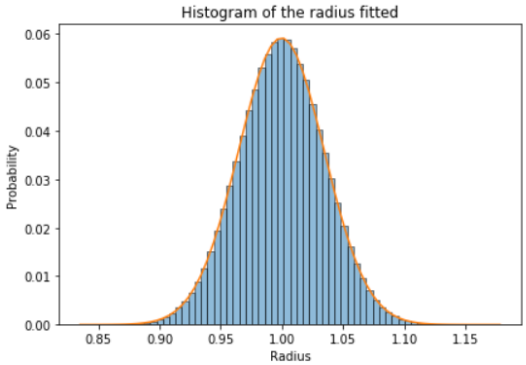

(a) A histogram of the radius fitted with a Gaussian distribution.

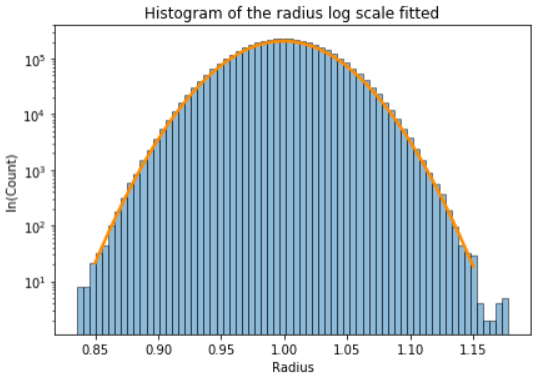

(b) The histogram of the radius on log scale with a parabola fitted.

Figure 5.11

Next to the histograms of the radius, also the histogram of the norm of the velocity can be made, figures 5.12a and 5.12b. These also show

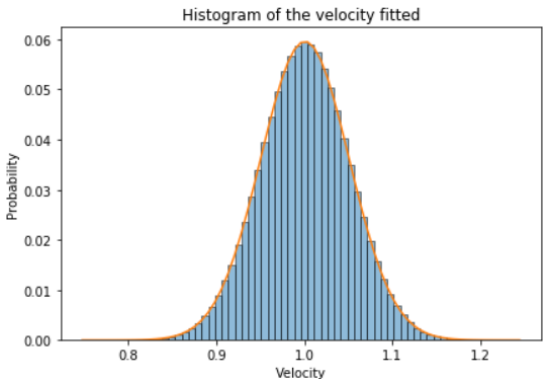

(a) A histogram of the velocity fitted with a Gaussian distribution.

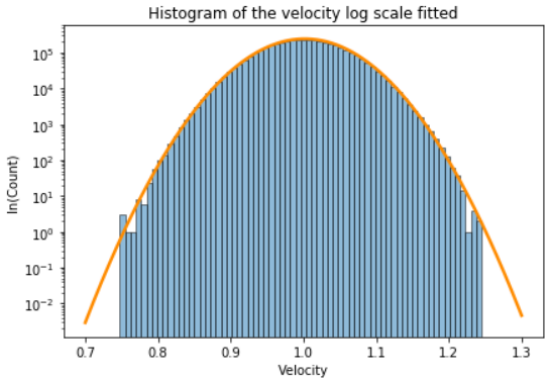

(b) The histogram of the velocity on log scale with a parabola fitted.

Figure 5.12

The average trajectory can also be calculated. In this case the trajectory was found by taking the the average over the radius for each angle. The result of that, see figure 5.13a, is as can be expected, the circle of radius 1 which was used as the target circle. Also the average velocity can be calculated in this way, see figure 5.13b, which is almost a straight line at 1.

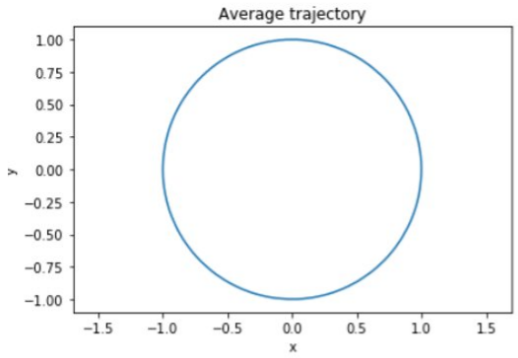

(a) The average trajectory of 1000 simulated trajectories.

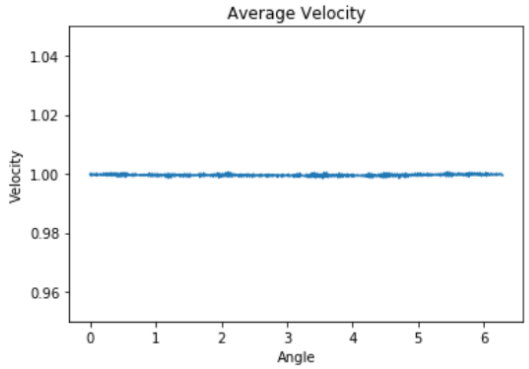

(b) The average velocity dependent on the angle.

Figure 5.13

6 Possible Applications

6.1 Modelling Real Pedestrians

To test the validity of the model the model has to be compared to real data. To do this a previously conducted experiment was taken and the model was used to make the simulations.

6.1.1 Real Data

The real data of pedestrians walking is taken from a previously conducted experiment [21] (Line crossings 2). It was chosen because the paths resemble a circular trajectory, which has been the running example for the model. The paths tough are not circles but closer to ellipses, so the model has to be tweaked to fit this. A schematic setup of the mean trajectory can be found in figure 6.14. The pedestrians are walking in only one direction, making the proposed model a good fit for this data.

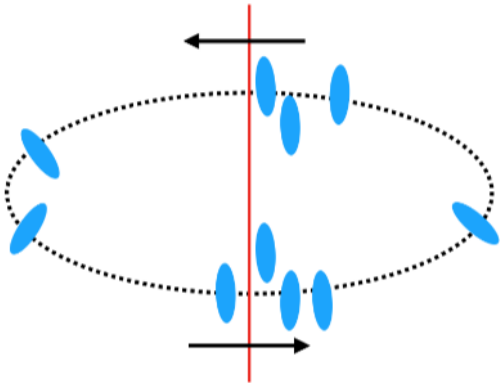

Figure 6.14: A schematic representation of the experiment conducted. Pedestrians (blue) are walking around in an ellipse (black dotted line) and fluctuating around the mean path [21].

Not all the data from this experiment is usable for the model. Besides noise and data from movement outside the experiment, there is also the fact that the pedestrians start in a single file and then, after about 1 minute, are told to group together. This make only the first minute compatible with the model as it is built for single, noninteracting pedestrians.

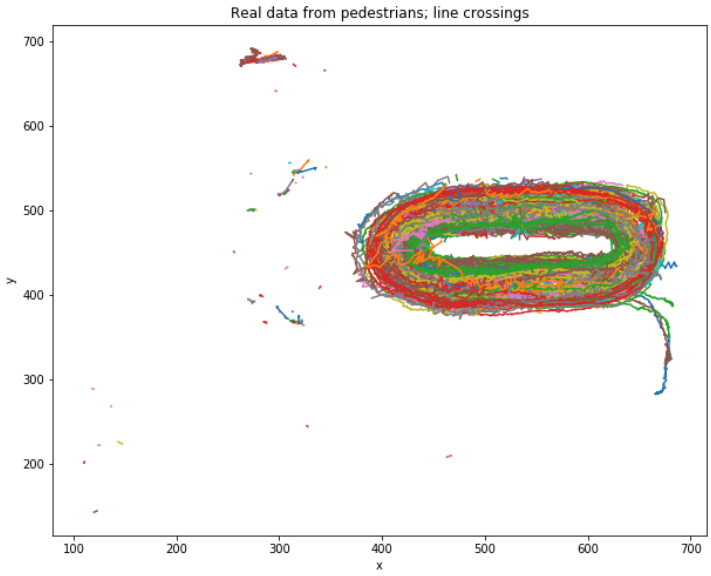

Figure 6.15: All the trajectories measured in the experiment before a selection was made for the usable trajectories.

After making a selection of the data and filtering out the very short trajectories, the remaining trajectories were translated to the origin of the coordinate system, figure 6.16.
The first step to take with this real data is to find the mean path. To do this, the angle and radius from the centre is calculated for each point,

$$r = \sqrt{x^2 + y^2} \quad \text{and} \quad \theta = \arctan\left(\frac{y}{x}\right). \tag{6.1}$$

Then for each angle an average over the radius is taken, resulting in the mean, or average, trajectory in figure 6.17. As expected, this mean resembles an ellipse and therefore, the next step is to fit an ellipse to the mean trajectory.
From the fit, the relevant parameters of the ellipse can be calculated, see table 1. These parameters can be used to make a proper model based on elliptical coordinates.

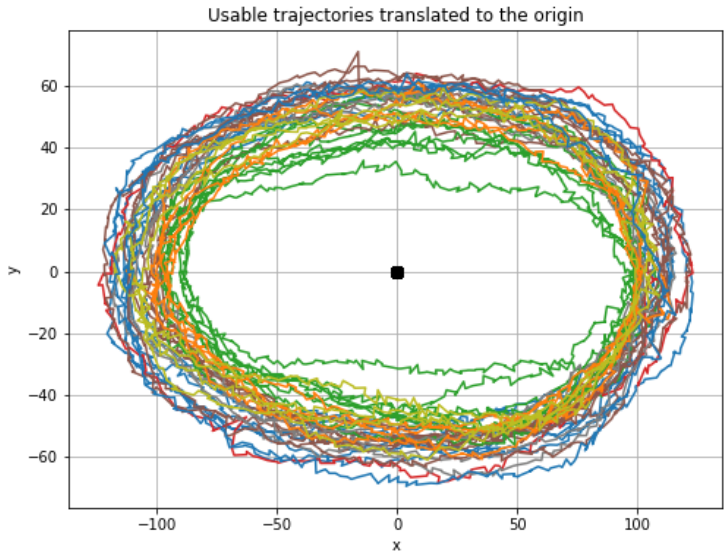

Figure 6.16: All the usable trajectories of the experiment translated to the origin and where the centre indicated by the black dot.

Semimajor axis a	106.87
Semiminor axis b	54.459
Eccentricity e	0.86042
Focal distance f	91.952

Table 1: The four important parameters of the fitted ellipse.

6.1.2 Elliptical Coordinates

To make the model for the data, an elliptical coordinate system is used, given by the mapping $(x, y) = \phi(\mu, \nu)$,

$$\phi : \begin{cases} x = a\cosh(\mu)\cos(\nu) \\ y = a\sinh(\mu)\sin(\nu) \end{cases} . \tag{6.2}$$

The prefactor a is the distance to the focal points and μ and ν the elliptical coordinates.
Using this transformation, the Jacobian,

$$J_\phi = a \begin{pmatrix} \sinh(\mu)\cos(\nu) & -\cosh(\mu)\sin(\nu) \\ \cosh(\mu)\sin(\nu) & \sinh(\mu)\sin(\nu) \end{pmatrix} \tag{6.3}$$

and its inverse,

$$J_\phi^{-1} = \frac{2}{a(\cos(2\nu) - \cosh(2\mu))} \begin{pmatrix} -\sinh(\mu)\cos(\nu) & -\cosh(\mu)\sin(\nu) \\ \cosh(\mu)\sin(\nu) & -\sinh(\mu)\sin(\nu) \end{pmatrix} \tag{6.4}$$

can be calculated. Using this, the Gaussian white noise can be transformed to the elliptical coordinate system as described in 3.2.6. Resulting in

$$\begin{pmatrix} \mathrm{d}\dot{\mu} \\ \mathrm{d}\dot{\nu} \end{pmatrix} = J_\phi^{-1} \circ \begin{pmatrix} W_x \\ W_y \end{pmatrix} \tag{6.5}$$

and by converting the back to Itô form, which surprisingly does not give any extra terms,

$$\begin{pmatrix} \mathrm{d}\dot{\mu} \\ \mathrm{d}\dot{\nu} \end{pmatrix} = J_\phi^{-1} \begin{pmatrix} W_x \\ W_y \end{pmatrix} . \tag{6.6}$$

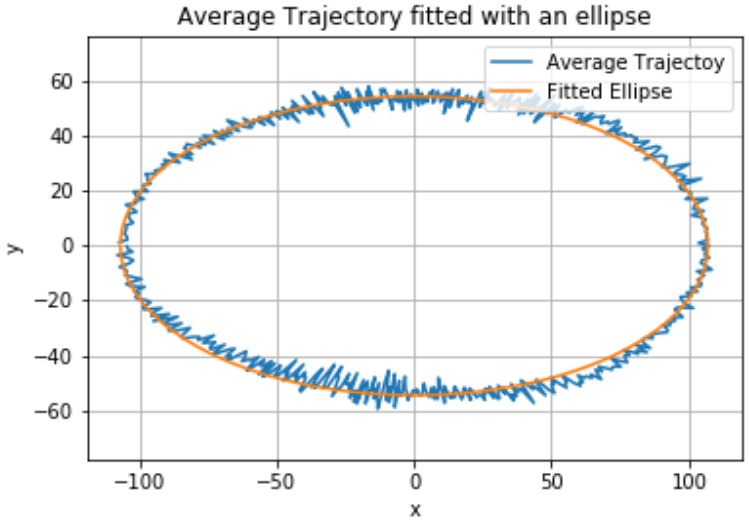

Figure 6.17: The calculated average trajectory (blue) and a fitted ellipse (orange) on top of that.

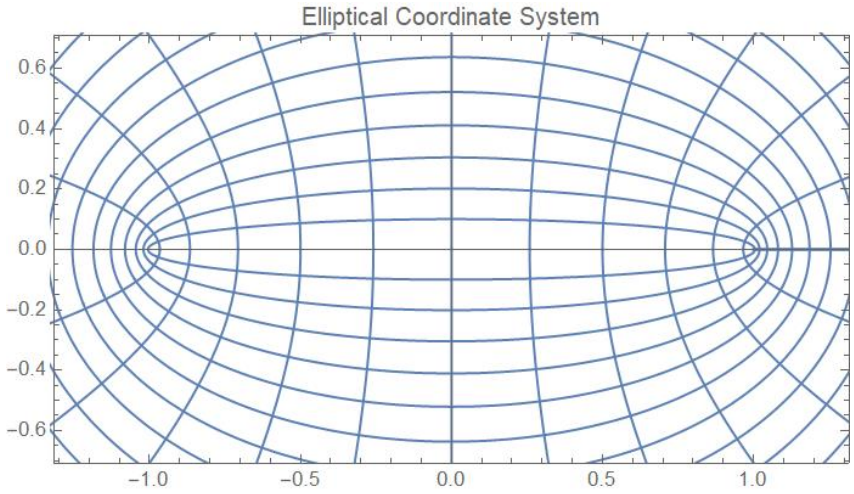

Figure 6.18: Coordinate lines of an elliptical coordinate system with $a = 1$. The ellipses are lines of constant μ and the hyperbola of constant ν.

To make the simulations, the model is made for elliptical coordinates. The focal point of the coordinate system are taken to be the same as those from the real , $a = 91.952$. The base equations are then given by

$$\begin{aligned} \ddot{\mu} &= 0 \\ \ddot{\nu} &= 0 \end{aligned} \quad . \tag{6.7}$$

Next, all the modelling components can be added, resulting in

$$\begin{cases} \dot{\mu} = u \\ \dot{\nu} = v \\ \dot{u} + \frac{v_{d\mu}\prime - u}{\tau} + \alpha(\mu - 0.5623) + \sigma W_\mu = 0 \\ \dot{v} + \frac{v_{d\nu}\prime - v}{\tau} + \sigma W_\nu = 0 \\ \dot{v}_{d\mu} = 0 \\ \dot{v}_\nu = 0 \end{cases} \quad . \tag{6.8}$$

Where a harmonic potential is put around the ellipse of $\mu = 0.5623$, the average of the experimental data. With all this in place, the simulated trajectories can be compared to the real ones.

6.1.3 Comparison Real and Simulated Trajectories

A first glance at the comparison of the experimental and simulated data, figure 6.19, shows that for single trajectories the visual correspondence fairly nice. Both trajectories exhibit the same type and size of fluctuations in the radial direction. The most obvious difference now is that the real data also has small, more frequent fluctuations in the trajectory. It probably is due to noise in the measurement. These should be able to be smoothed out with a smoothing function if so desired.

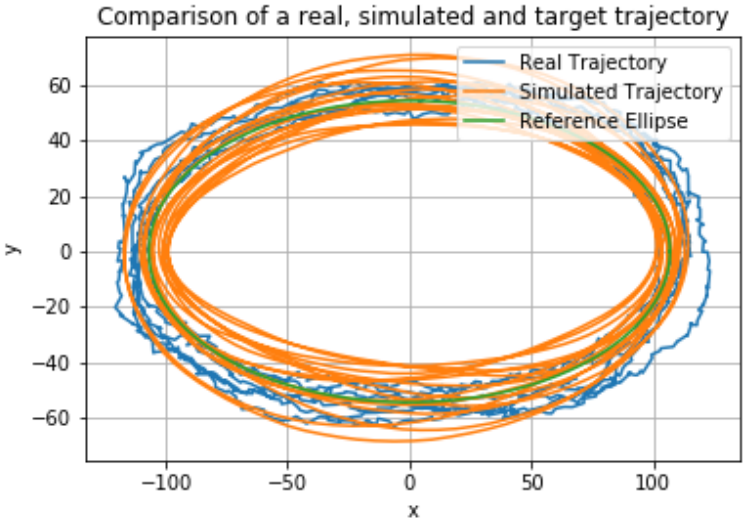

Figure 6.19: A comparison between a real (blue line) and a simulated trajectory (orange line) with the desired path (green line) added in.

One of the things that can be done to numerically compare the experiment to the simulation is to make a probability density function (pdf) of the μ coordinate and compare those. As can be seen in figure 6.20, the distributions are very similar to one another. Meaning that the model has a good approximate distribution in the μ coordinate.

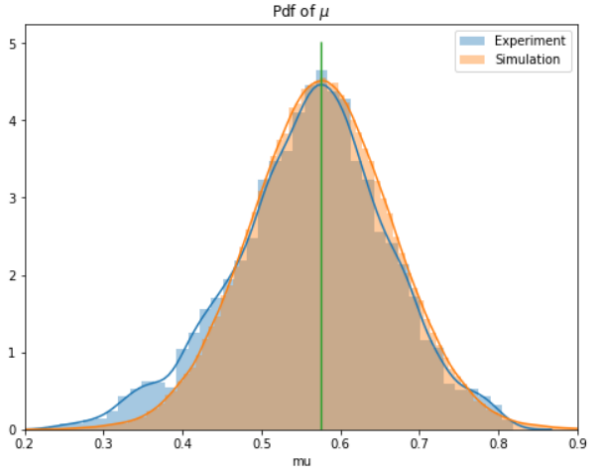

Figure 6.20: The pdf of μ for both the experimental and the simulated trajectories.

One thing of notice in figure 6.20 is that there are two slight bumps on either side of the peak near the bottom. These do not follow the normal Gaussian distribution. This can also be seen in the figure 6.21, where smaller ellipse coincides with the green trajectory and the largest ellipse with the outermost trajectories on the right and left side. These bumps can be due to the fact that the experimental data set is on the small side and that thus the outlying trajectories weigh in heavily on the distribution.

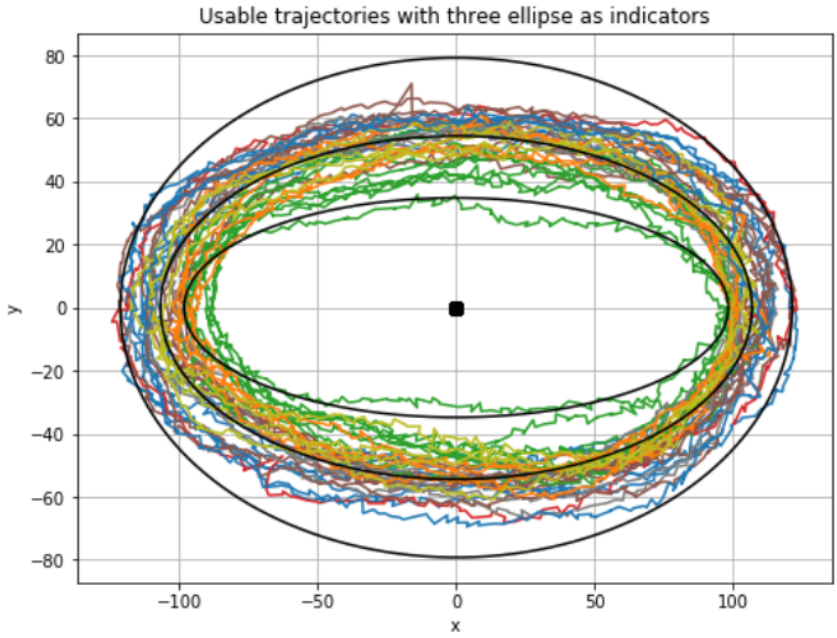

Figure 6.21: The usable trajectories as show in 6.16 with thee ellipses plotted on top located at the large peak and the two bumps of the distribution plot, figure 6.20

The velocity component $\dot{\mu}$, see figure 6.22, exhibits a pdf centred around 0, as expected. And once again shows two bumps near the bottom that differ. These are probably caused by the fact that the average trajectory of the experimental data is not a perfect ellipse, as can be seen in figure 6.17. The slight deviations in- and outwards may be the cause of the two bumps. As there are a few points where, on average, $\dot{\mu} \neq 0$, that may cause the slight deviations.
Both of the fits themselves not perfect, but this can be improved with proper parameter fitting, instead of adjusting a human guess.

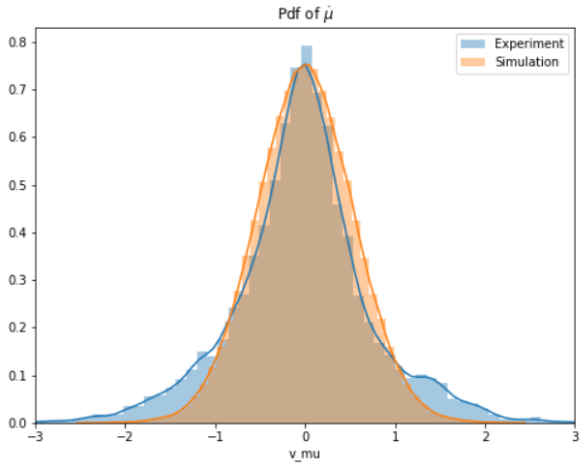

Figure 6.22: The pdf of $\dot{\mu}$ for both the experimental and the simulated trajectories with $\epsilon = 9.337$, $\alpha = 16.05$, $\tau = 10.2$.

6.2 Improvements in the Model

6.2.1 Energy Conservation

There are some improvements that can be made in the model. First is to, similarly as was done in the circular example, conserve the total kinetic energy T,

$$T = g_{ij}\dot{q}^i\dot{q}^j, \tag{6.9}$$

where,

$$g_{ij} = \begin{pmatrix} 1 & 0 \\ 0 & 1 \end{pmatrix} \tag{6.10}$$

in Cartesian coordinates and should be considered as normal, i.e. not defined by the new connection. To not implement this may cause some problems when the deviations get very large as the energy would not be conserved.

6.2.2 Varying Desired velocity

Another interesting improvement can be found in taking the desired to not be a constant. A function with time or spatial dependence could be used instead,

$$\vec{v}_d = \vec{v}_d(\vec{q}, t). \tag{6.11}$$

The action of rescaling would remain the same as discussed in section 4.5. This idea might be used to make a pedestrian start running at a certain time, or to have them slow down when walking uphill.

6.3 Further Outlook

An important question is; What can be done with this model? The possibilities are quite numerous, so a few options are given here and some possible ideas on how to realise them.

6.3.1 Simulations Based on Experiments

To expand on the previous section, the model can be used to make simulations out of real experiments. This can be done, in easy cases, by taking the mean path of experimental data, like done before, and defining that as a geodesic. From this geodesic, a coordinate system can be constructed [22, 23, 24]. With this coordinate system, the model can be made and simulations can be run, either to verify the model works or to actually use it as a simulation.

6.3.2 Interacting Pedestrians

The model here is designed for single pedestrians walking along a path. Though in the cities or train stations the interesting cases happen when multiple pedestrians are interacting with each other. This could be integrated into the model by giving each pedestrian a potential around them. That, for example, person A and B both have a potential of Gaussian shape around them and that, when they come closer to each other the potentials push them away again. This can be viewed similar to the pairwise avoidance model [25].

6.3.3 Obstructions and Guiding

Similar to giving persons a potential, objects like walls or pillars etc. can be given a potential. and that way the pedestrians are not only walking in a harmonic potential but also a potential created by their surroundings. This could be used when designing escape routes, by carefully placing objects that guide the pedestrian to the exit.

In the same line of thinking, also time dependent potentials can be introduced, think about traffic lights or revolving doors, that can influence the paths of the pedestrians.

7 Conclusions

In this thesis, a new model for pedestrian dynamics was introduced. This model uses differential geometry to describe curved force free paths. These paths are used as the target trajectories of pedestrians. With the modelling components like the potential, active friction and random noise, trajectories of pedestrians can be simulated. When an average is taken over many of these trajectories, the initial curved path that was used to make the model is recovered. The distribution of the orthogonal coordinate to the path, that should be constant, is Gaussian as designed. As is the distribution of the norm of velocity.

In a brief comparison to experimental data, it was found that the simulated trajectories are corresponding very well to the real ones. And the distributions of the constant coordinate and its time derivative are very similar as well, up to some discrepancies. In addition, a few improvements and uses for the model are suggested.

To conclude, the model put forth is by no means perfect, but it show good results and even a small comparison with experimental data is very promising. Meaning that, when the model is further tested and improved with real data, it can be used to predict behaviours of pedestrians. Which in turn can be used to design escape routes from buildings or walkways through a city.

8 Acknowledgements

I would like to thank my supervisors prof. F. Toschi and dr. A. Corbetta for their consistent support and guidance during the running of this project. Without them it would not have become the thesis it is now.

A Appendix

https://github.com/ArthurGrootZevert/Cuvilinear-Pedestrian-Dynamics/

Simulation	**Type**	**Path**
Conserved Angular Velocity	Script	`const_angular_velo_with_confinement.ipynb`
Conserved Angular Momentum	Script	`const_angular_momentum_with_confinement.ipynb`
Statistics on Circle	Script	`xyandr,thdatastatisticssolvedwithitoint.ipynb`
Experimental Data	Real Paths	`dataframe`
	Simulated Paths	`Elliptical_simulations`
	Script	`Realdatacomparisonwiththemodel.ipynb`

References

[1] Pushkin Kachroo. *Pedestrian Dynamics: Mathematical Theory and Evacuation Control*. 1 2010.

[2] John Zacharias. Modeling pedestrian dynamics in Montreal's underground city. Technical report.

[3] John Zacharias. Planning Underground Urban Space-Where, When and How? Technical report.

[4] Claudio Castellano, Santo Fortunato, and Vittorio Loreto. Statistical physics of social dynamics. 10 2007.

[5] Ioannis Karamouzas, Brian Skinner, and Stephen J Guy. Universal Power Law Governing Pedestrian Interactions. *Physical Review Letters*, 113(23):238701, 12 2014.

[6] Dirk Hartmann. Adaptive pedestrian dynamics based on geodesics. *New Journal of Physics*, 12(4):043032, 4 2010.

[7] Peng Wang and Peter Luh. Fluid-Based Analysis of Pedestrian Crowd at Bottlenecks. 9 2013.

[8] Nicolas Bain and Denis Bartolo. Dynamic response and hydrodynamics of polarized crowds. *Science*, 363(6422):46, 1 2019.

[9] Dirk Helbing. A Fluid Dynamic Model for the Movement of Pedestrians. 5 1998.

[10] Alessandro Corbetta, Chung Min Lee, Roberto Benzi, Adrian Muntean, and Federico Toschi. Fluctuations around mean walking behaviors in diluted pedestrian flows. *Physical Review E*, 95(3), 3 2017.

[11] Theodore Frankel. *The Geometry of Physics: An Introduction*. Cambridge University Press, Cambridge, 2 edition, 2003.

[12] Florian Herzog. Stochastic Differential Equations. Technical report, 2013.

[13] Brownian Motion and Stochastic Differential Equations. Technical report.

[14] Michael Hauser. The Derivative of Brownian Motion is White Gaussian Noise. Technical report.

[15] Gregory Chirikjian. *Stochastic Models, Information Theory, and Lie Groups, Volume 1: Geometry of curves and surfaces*. Birkhäuser Boston, 5 2009.

[16] Yousef S Ali Alnafisah. First-order Numerical Schemes for Stochastic Differential Equations Using Coupling. Technical report, 2015.

[17] Yousef Alnafisah. The Implementation of Milstein Scheme in Two-Dimensional SDEs Using the Fourier Method. *Abstract and Applied Analysis*, 2018, 2018.

[18] Gisiro Maruyama. Continuous Markov processes and stochastic equations. *Rendiconti del Circolo Matematico di Palermo*, 4(1):48, 1955.

[19] Peter Kloeden and Eckhard Platen. Numerical Solution of Stochastic Differential Equations. pages 1–50. 1 1992.

[20] Andreas Rößler. Runge-Kutta methods for the strong approximation of solutions of stochastic differential equations. *SIAM Journal on Numerical Analysis*, 48(3):922–952, 2010.

[21] J A Willems dr Corbetta prof F Toschi. Quantifying the quality of pedestrian trajectory measurements: ProRail consultancy report. Technical report, 2019.

[22] Vladimir E Zakharov. Description of the n-orthogonal curvilinear coordinate systems and hamiltonian integrable systems of hydrodynamic type, i: integration of the lamlk equations. Technical Report 1, 1998.

[23] I Krichever. Algebraic-geometrical n-orthogonal curvilinear coordinate systems and solutions to the associativity equations. Technical report, 1996.

[24] A. E. Mironov and I. A. Taimanov. Orthogonal curvilinear coordinate systems corresponding to singular spectral curves. In *Proceedings of the Steklov Institute of Mathematics*, volume 255, pages 169–184, 12 2006.

[25] Alessandro Corbetta, Jasper Meeusen, Chung-min Lee, roberto benzi, and Federico Toschi. *Physics-based modeling and data representation of pedestrian pairwise interactions.* 8 2018.